symmetry

MDPI

Article

Associated Charmonium-Bottomonium Production in a Single Boson e^+e^- Annihilation

Ilia Belov [1,2,*], Alexander Berezhnoy [1] and Evgeny Leshchenko [2]

[1] Skobeltsyn Institute of Nuclear Physics, Moscow State University, 119991 Moscow, Russia; Alexander.Berezhnoy@cern.ch
[2] Physics Department, Moscow State University, 119991 Moscow, Russia; leshchenko.ea17@physics.msu.ru
* Correspondence: Ilia.Belov@cern.ch

Abstract: The production cross sections of $J/\psi\,\eta_b$, $\Upsilon\,\eta_c$ pairs in a single boson e^+e^- annihilation have been studied in a wide range of energies, which will be achieved at future e^+e^- colliders. The main color singlet contributions to the production processes are taken into account, including the one loop QCD contribution.

Keywords: e^+e^- interactions; heavy quarks; quarkonium production; NRQCD; one loop contributions

Citation: Belov, I.; Berezhnoy, A.; Leshchenko, E. Associated Charmonium-Bottomonium Production in a Single Boson e^+e^- Annihilation. *Symmetry* **2021**, *13*, 1262. https://doi.org/10.3390/sym13071262

Academic Editor: Dmitri Melikhov

Received: 11 June 2021
Accepted: 9 July 2021
Published: 15 July 2021

1. Introduction

Despite its long history, heavy quark physics continues to attract the attention of both theorists and experimentalists. Recently, due to the LHC experiments, almost every year, the BELLE-II experiment and the BES-III experiment is marked by a discovery in this area. One of the hot topics of research is quarkonium pair production. It is worth noting here the intrigue related to the observation of $J/\psi\,\eta_c$ pair in the e^+e^- annihilation: the theoretical predictions [1] underestimated the real yield measured at BELLE and BaBar [2,3] by the order of magnitude. This stimulated numerous studies [4–21], as a result of which a fair agreement with the data has been achieved. The previous year gave researchers a new sensation: the LHCb Collaboration observed the structure in the $J/\psi\,J/\psi$ spectrum at large statistics [22]. This circumstance led to a real explosion of interest towards this topic.

Looking to the future, we study the processes of paired quarkonium production which can not be observed at the existing experiments due to low interaction energy, namely, the production of $J/\psi\,\eta_b$ pairs and $\Upsilon\,\eta_c$ pairs in the e^+e^- annihilation. These processes can be investigated in the framework of several discussed projects: ILC, FCC, and the muon collider. At ILC and FCC, studies are planned at the energies of the order of Z-boson's mass: the energy range announced for FCC is $\sqrt{s} = 90 \div 400$ GeV [23] and $\sqrt{s} = 250$ GeV is proposed for ILC [24]. In the project of muon collider, it is planned to implement the $\mu^+\mu^-$ collisions at energies from 3 TeV to 14 TeV [25], which are beyond the energy range studied in this work.

It is worthy to note that the decays of Z-boson to the charmonium and the bottomonium may be of some interest for the experiments at the LHC, see [26].

In our previous studies, we already investigated the paired B_c production [27], as well as the $J/\psi\,J/\psi$ and the $J/\psi\,\eta_c$ pair production around the Z mass within the NLO approximation [28]. We found that for these processes the loop corrections essentially contribute to the cross section values. This result is in agreement with the studies of other research groups investigated the paired quarkonium production in the e^+e^- annihilation. Both cases of $J/\psi\,\eta_b$ and $\Upsilon\,\eta_c$ production are special, because the tree level diagrams with the single gluon exchange can not contribute to the production of $c\bar{c}$ and $b\bar{b}$ pairs in the color singlet states, and therefore the lowest order QCD contribution to these processes contains loops. This one-loop contribution is of the order of $\mathcal{O}(\alpha^2\alpha_s^4)$, that is why it makes

sense to investigate it with the purely electromagnetic $J/\psi\ \eta_b$ and $\Upsilon\ \eta_c$ production which is of the order of $\mathcal{O}(\alpha^4)$, since $\alpha_s^2 \sim \alpha$.

When studying these processes, one cannot ignore the discussion of the role of color octet contributions. Indeed, from one side the paired color octet production is suppressed as $v_{c\bar{c}}^2 v_{b\bar{b}}^2 \sim 0.03$, where $v_{c\bar{c}}$ and $v_{b\bar{b}}$ are velocities of quarks inside charmonium and botomonium, correspondingly. From the other side, it has no additional suppression by α_s^2, going through the tree level QCD diagrams. Therefore, a color octet mechanism could essentially contribute to the discussed quarkonium-pair production. It deserves a separate detailed consideration, which goes beyond the scope of the current study.

Another problem that is outside the scope of this study is the relativistic effects caused by the use of relativistic or relativized wave functions. It is known that accounting for such effects can crucially change the predictions, especially for the charmonium-pair production in the e^+e^- annihilation, where accounting for the relativistic effects decreases the virtuality of the intermediate gluon, and therefore essentially increases the cross section value (see for example [9–21]). Another example of the influence of the relativistic effects on the paired quarkonium production could be found in [29–32]. For the processes discussed in this study, we do not expect such a huge change of the cross section due to relativistic effects, as for the paired charmonium production, but, of course, it does not eliminate the problem, and such effects should be thoroughly investigated.

It is worth mentioning that the one loop QCD diagrams do not contribute to the production of J/ψ Υ-pair in a single boson e^+e^--annihilation. In leading order, such a process goes via the electroweak Z boson decay only. As we planned the current work as a continuation of our previous studies on the one loop QCD corrections, in a sense, this process is slightly out of our interest. However, we keep it in our consideration for comparison with $J/\psi\ \eta_b$ and $\Upsilon\ \eta_c$ production. Thus, the following processes are considered in this study:

$$\begin{cases} e^+e^- \xrightarrow{\gamma^*,\, Z^*} J/\psi\ \eta_b, \\ e^+e^- \xrightarrow{\gamma^*,\, Z^*} \Upsilon\ \eta_c, \\ e^+e^- \xrightarrow{Z^*} J/\psi\ \Upsilon. \end{cases} \tag{1}$$

2. Calculation Technique

The production of the pair of charmonium and bottomonium in a single boson annihilation is constrained by several selection rules, which are discussed below.

The production of the J/ψ Υ pairs is not allowed in the photon exchange, as well as it does not go via the vector part of Z vertex due to the charge parity conservation. The J/ψ Υ pairs are produced via the interaction with the axial part of Z vertex only. As concerned the $\eta_b\ \eta_c$ pair production, it goes neither via the photon exchange, nor via the Z-boson exchange: the photon decay to the $\eta_b\ \eta_c$ pair is forbidden due to the charge parity conservation, and the Z decay to the $\eta_b\ \eta_c$ pair is forbidden due to the combined CP parity conservation. At the same time, the vector-pseudoscalar (VP) pairs: $J/\psi\ \eta_b$ and $\Upsilon\ \eta_c$ are produced via the exchange of both the photon and the Z-boson. These selection rules were reproduced directly in our calculations.

As we already pointed out in the Introduction, the tree level diagrams describing the single gluon exchange do not contribute to the discussed processes, and the lowest order QCD contribution to such processes contains loops. This one-loop QCD contribution is of the order of $\mathcal{O}(\alpha^2\alpha_s^4)$ and therefore it could be comparable with the pure electroweak tree level contribution, which is of the order of $\mathcal{O}(\alpha^4) \sim \mathcal{O}(\alpha^2\alpha_s^4)$. Thus, when studying these processes, one should take into account the electroweak contribution (EW) of the order of $\mathcal{O}(\alpha^4)$, the one loop QCD contribution of the order of $\mathcal{O}(\alpha^2\alpha_s^4)$, and the interference between them of the order of $\mathcal{O}(\alpha^3\alpha_s^2)$:

$$|\mathcal{A}|^2 = |\mathcal{A}^{EW}|^2 + 2Re(\mathcal{A}^{EW}\mathcal{A}^{QCD*}) + |\mathcal{A}^{QCD}|^2. \tag{2}$$

For the more detailed study of the processes we consider the amplitudes with different intermediate bosons separately:

$$|\mathcal{A}|^2 = |\mathcal{A}_\gamma^{EW}|^2 + |\mathcal{A}_Z^{EW}|^2 + 2Re(\mathcal{A}_\gamma^{EW}\mathcal{A}_Z^{EW*}) + \\ + 2Re(\mathcal{A}_\gamma^{EW}\mathcal{A}_\gamma^{QCD*}) + 2Re(\mathcal{A}_Z^{EW}\mathcal{A}_Z^{QCD*}) + 2Re(\mathcal{A}_\gamma^{EW}\mathcal{A}_Z^{QCD*}) + 2Re(\mathcal{A}_Z^{EW}\mathcal{A}_\gamma^{QCD*}) + \\ + |\mathcal{A}_\gamma^{QCD}|^2 + |\mathcal{A}_Z^{QCD}|^2 + 2Re(\mathcal{A}_\gamma^{QCD}\mathcal{A}_Z^{QCD*}). \quad (3)$$

The production of double heavy quarkonia is described in the framework of nonrelativistic QCD (NRQCD). This formalism allows us to factor out the perturbative degrees of freedom and therefore separate the production mechanism into hard and soft subprocesses, using the hierarchy of scales for the quarkonia, which is $m_q >> m_q v,\ m_q v^2, \Lambda_{QCD}$, where m_q is the heavy quark mass and v is the velocity of heavy quark in the quarkonium. The hard subprocess corresponds to the perturbative production of $q\bar{q}$-pair, while the soft subprocess corresponds to the fusion of quarks into the bound state.

To compute the matrix elements for the studied processes, we start from the matrix element for $e^+e^- \to c(p_c)\bar{c}(p_{\bar{c}})b(p_b)\bar{b}(p_{\bar{b}})$ with heavy quarks and antiquarks on their mass shells: $p_c^2 = p_{\bar{c}}^2 = m_c^2$ and $p_b^2 = p_{\bar{b}}^2 = m_{\bar{b}}^2$. As we put $v = 0$ before the projection onto the bound states, the momentum P of charmonium and the momentum Q of bottomonium are related with the heavy quark momenta as follows:

$$J/\psi,\ \eta_c \begin{cases} p_c = P/2 \\ p_{\bar{c}} = P/2 \end{cases} \qquad \Upsilon,\ \eta_b \begin{cases} p_b = Q/2 \\ p_{\bar{b}} = Q/2 \end{cases} \quad (4)$$

To construct the bound states we replace the spinor products $v(p_{\bar{q}})\bar{u}(p_q)$ by the appropriate covariant projectors for color-singlet spin-singlet and spin-triplet states:

$$\Pi_{J/\psi}(P, m_c) = \frac{\not{P} - 2m_c}{2\sqrt{2m_c}} \not{\epsilon}^{J/\psi} \otimes \frac{\mathbf{1}}{\sqrt{N_c}}, \qquad \Pi_{\eta_c}(P, m_c) = \frac{\not{P} - 2m_c}{2\sqrt{2m_c}} \gamma^5 \otimes \frac{\mathbf{1}}{\sqrt{N_c}}, \quad (5)$$

$$\Pi_{\Upsilon}(Q, m_b) = \frac{\not{Q} - 2m_b}{2\sqrt{2m_b}} \not{\epsilon}^{\Upsilon} \otimes \frac{\mathbf{1}}{\sqrt{N_c}}, \qquad \Pi_{\eta_b}(Q, m_b) = \frac{\not{Q} - 2m_b}{2\sqrt{2m_b}} \gamma^5 \otimes \frac{\mathbf{1}}{\sqrt{N_c}}, \quad (6)$$

where $\epsilon^{J/\psi}$ and ϵ^{Υ} are the polarizations of the J/ψ and Υ mesons, satisfying the following constraints: $\epsilon^{J/\psi} \cdot \epsilon^{J/\psi *} = -1$, $\epsilon^{J/\psi} \cdot P = 0$, $\epsilon^{\Upsilon} \cdot \epsilon^{\Upsilon *} = -1$ and $\epsilon^{\Upsilon} \cdot Q = 0$.

These operators close the fermion lines into traces. The examples of diagrams contributing to the process $e^+e^- \to J/\psi\,\eta_b$ are shown in Figure 1.

The factorized matrix elements have the following form:

$$\mathcal{A}(e^+e^- \to J/\psi\,\eta_b) = \frac{\langle O_{J/\psi}\rangle^{1/2}\langle O_{\eta_b}\rangle^{1/2}}{N_c} \mathcal{M}^{\mu}_{J/\psi\,\eta_b} \epsilon^{J/\psi}_{\mu}, \quad (7)$$

$$\mathcal{A}(e^+e^- \to \Upsilon\,\eta_c) = \frac{\langle O_{\Upsilon}\rangle^{1/2}\langle O_{\eta_c}\rangle^{1/2}}{N_c} \mathcal{M}^{\mu}_{\Upsilon\,\eta_c} \epsilon^{\Upsilon}_{\mu}, \quad (8)$$

$$\mathcal{A}(e^+e^- \to J/\psi\,\Upsilon) = \frac{\langle O_{J/\psi}\rangle^{1/2}\langle O_{\Upsilon}\rangle^{1/2}}{N_c} \mathcal{M}^{\mu\nu}_{J/\psi\,\Upsilon} \epsilon^{J/\psi}_{\mu} \epsilon^{\Upsilon}_{\nu}, \quad (9)$$

where $\mathcal{M}^{\mu}_{J/\psi\,\eta_b}$, $\mathcal{M}^{\mu}_{\Upsilon\,\eta_c}$, and $\mathcal{M}^{\mu\nu}_{J/\psi\,\Upsilon}$ are the hard production amplitudes of two quark-antiquark pairs projected onto the quark-antiquark states with zero relative velocities and the appropriate quantum numbers by projectors (5) and (6). The NRQCD matrix elements $\langle O_{\Upsilon}\rangle$, $\langle O_{J/\psi}\rangle$, $\langle O_{\eta_b}\rangle$ and $\langle O_{\eta_c}\rangle$ are vacuum-saturated analogs of the NRQCD matrix elements $\langle O(^3S_1)\rangle$ and $\langle O(^1S_0)\rangle$ for annihilation decays defined in [33]. The numerical values of these matrix elements can be estimated from the experimental data on decays [1,34,35], or adopted from the potential models, such as [36], using the relation $\langle O\rangle \approx \frac{N_c}{2\pi}|R(0)|^2$, where $R(0)$ is the quarkonium wave function at origin (see Table A1 of Appendix A).

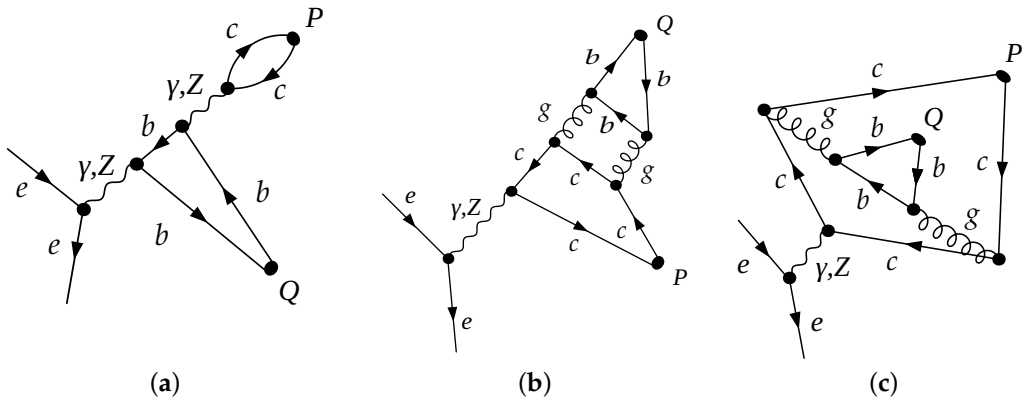

Figure 1. The diagram examples contributing to the $e^+e^- \to J/\psi\, \eta_b$ process: the tree level electroweak diagram (**a**); the diagrams with a QCD loop (**b**,**c**).

3. Workflow

The diagrams and the corresponding analytic expressions are generated with the `FeynArts`-package [37] in Wolfram Mathematica. The electroweak contribution to the production amplitudes is determined by the tree diagrams of type (a) shown in Figure 1, whereas the one-loop diagrams of type (b) and (c) contribute to the QCD amplitudes.

We obtain 4 nonzero electroweak and 6 nonzero QCD diagrams for each subprocesses $e^+e^- \xrightarrow{\gamma^*} J/\psi\, \eta_b$, $e^+e^- \xrightarrow{Z^*} J/\psi\, \eta_b$, $e^+e^- \xrightarrow{\gamma^*} \Upsilon\, \eta_c$ and $e^+e^- \xrightarrow{Z^*} \Upsilon\, \eta_c$. The associative production of two vector states J/ψ and Υ is described only by the tree electroweak diagrams of type (a). These results, as well as the explicitly obtained zero contribution to the process of $\eta_b\, \eta_c$ production, are in exact agreement with the earlier discussed selection rules, providing the additional verification of the procedure.

To calculate the tree level amplitudes we use only `FeynArts` [37] and `FeynCalc` [38] packages in `Wolfram Mathematica`, while the computation of the one loop amplitudes requires a more complicated toolchain: `FeynArts` $\to$ `FeynCalc(TIDL)` $\to$ `Apart` [39]$\to$ `FIRE` [40]$\to$ `X` [41].

All necessary algebraic calculations with Dirac and colour matrices, including the trace evaluation, were performed within the `FeynCalc` package. At the next step the Passarino-Veltman reduction is carried out using the `TIDL` library implemented in `FeynCalc`. The `Apart` function does the extra simplification by partial fractioning for IR-divergent integrals. The `FIRE` package provides the complete reduction of the integrals obtained in the previous stages to master integrals. This package implements several strategies for the IBP reduction mostly based on the Laporta algorithm [42]. The master integrals are then evaluated by substitution of their analytical expressions with the help of `X`-package.

The conventional dimensional regularization (CDR) scheme with D-dimensional loop and external momenta is used to compute the QCD amplitudes. Each QCD amplitude for the separate loop diagram carries a singular term of the order of $\mathcal{O}(1/\varepsilon)$. These terms cancel out after summing over the set of QCD amplitudes, as expected.

It is known that γ^5 is poorly defined in D-dimensions. In the current study, the so-called naive interpretation of γ^5 was used: γ^5 anticommutes with all other matrices and therefore disappears in traces with an even number of γ^5. In traces with an odd number of γ^5 the remaining γ^5 is moved to the right and replaced by

$$\gamma^5 = \frac{-i}{24}\varepsilon_{\alpha\beta\sigma\rho}\gamma^\alpha\gamma^\beta\gamma^\sigma\gamma^\rho. \tag{10}$$

Since $\varepsilon_{\alpha\beta\sigma\rho}$ is contracted after the regularization procedure, we can safely treat it as 4-dimensional.

4. Analytical Form of the Amplitudes

The relative simplicity of the considered processes makes it possible to provide the analytical expressions for the amplitudes right in the text.

The electroweak amplitudes for the processes $e^+e^- \to J/\psi\,\eta_b$ and $e^+e^- \to \Upsilon\,\eta_c$ can be written as per

$$\mathcal{A}_{EW}\left(e^+e^- \to J/\psi\,\eta_b\right) = \frac{\langle O_{J/\psi}\rangle^{1/2}\langle O_{\eta_b}\rangle^{1/2}}{N_c}\times \\ \times \frac{-e^4\,e_b e_c}{2N_c m_c\sqrt{m_b m_c}\,\left(s+4m_c^2-4m_b^2\right)}\left(b_\gamma J_\mu + b_Z\widetilde{J}_\mu\right)\epsilon_\nu^{J/\psi}P_\rho Q_\sigma \varepsilon^{\mu\nu\rho\sigma}. \quad (11)$$

$$\mathcal{A}_{EW}\left(e^+e^- \to \Upsilon\,\eta_c\right) = \frac{\langle O_\Upsilon\rangle^{1/2}\langle O_{\eta_c}\rangle^{1/2}}{N_c}\times \\ \times \frac{e^4\,e_b e_c}{2N_c m_b\sqrt{m_b m_c}\,\left(s+4m_b^2-4m_c^2\right)}\left(c_\gamma J_\mu + c_Z\widetilde{J}_\mu\right)\epsilon_\nu^{\Upsilon}P_\rho Q_\sigma \varepsilon^{\mu\nu\rho\sigma}, \quad (12)$$

where $e_c = 2/3$ and $e_b = -1/3$ are the quark charges, J_μ and $\widetilde{J}$ are the parts of electroweak current which describe the e^+e^- annihilation to the virtual photon and to the virtual Z boson correspondingly ($J_\mu = -i\,\bar{e}\gamma_\mu e$, $\widetilde{J}_\mu = -i\,\bar{e}\,\Gamma_\mu^Z e$), and

$$c_\gamma = \frac{4e_c}{s}, \qquad c_Z = \left(\frac{4e_c\sin^2\theta_w - 1}{\cos\theta_w\sin\theta_w}\right)\frac{1}{s-M_Z^2+i\Gamma M_Z}, \quad (13)$$

$$b_\gamma = \frac{4e_b}{s}, \qquad b_Z = \left(\frac{4e_b\sin^2\theta_w + 1}{\cos\theta_w\sin\theta_w}\right)\frac{1}{s-M_Z^2+i\Gamma M_Z}. \quad (14)$$

Such a simple structure of amplitudes (11) and (12) is explained by the fact that only the vector, i.e., the photon-like part of $Zq\bar{q}$ vertex contributes to the decays $Z^* \to J/\psi\,\eta_b$ and $Z^* \to \Upsilon\,\eta_c$.

The analytical expressions for the cross sections of the electromagnetic production of $J/\psi\,\eta_b$ and $\Upsilon\,\eta_c$ pairs via the photon exchange are very simple and thus might be shown in the text:

$$\sigma_{QED}\left(e^+e^- \xrightarrow{\gamma^*} J/\psi\,\eta_b\right) = \\ = \frac{32\pi^3\alpha^4 e_b^4 e_c^2 \mathcal{O}_{\eta_b}\mathcal{O}_{J/\psi}\left(16m_b^4 - 8m_b^2\left(4m_c^2+s\right) + \left(s-4m_c^2\right)^2\right)^{3/2}}{3m_b m_c^3 N_c^4 s^3\left(-4m_b^2+4m_c^2+s\right)^2}, \quad (15)$$

$$\sigma_{QED}\left(e^+e^- \xrightarrow{\gamma^*} \Upsilon\,\eta_c\right) = \\ = \frac{32\pi^3\alpha^4 e_c^4 e_b^2 \mathcal{O}_{\eta_c}\mathcal{O}_{\Upsilon}\left(16m_c^4 - 8m_c^2\left(4m_b^2+s\right) + \left(s-4m_b^2\right)^2\right)^{3/2}}{3m_c m_b^3 N_c^4 s^3\left(-4m_c^2+4m_b^2+s\right)^2}. \quad (16)$$

It should be noted that in the $e^+e^- \to J/\psi\,\eta_b$ and $e^+e^- \to \Upsilon\,\eta_c$ processes the virtual photon transforming into the vector meson ($\gamma^* \to J/\psi$ or $\gamma^* \to \Upsilon$, see picture (a) in Figure 1) can be complemented by the analogous processes with Z boson. Formally, all theses processes are of the same order in terms of coupling constants. However the latter ones are extremely suppressed by the Z boson propagator as factors $\left(\frac{m_c^2}{M_Z^2-4m_c^2}\right)$ and

$\left(\frac{m_b^2}{M_Z^2-4m_b^2}\right)$, correspondingly, and can be neglected. The analytical expressions for these contributions can be found in (A1) and (A2) of Appendix B.

The QCD one loop contributions to the amplitudes of the discussed processes have exactly the same Lorentz structure as the electroweak contributions (11) and (12):

$$\begin{aligned}
\mathcal{A}_{QCD}\left(e^+e^- \to J/\psi\,\eta_b\right) = {} & \frac{\langle O_{J/\psi}\rangle^{1/2}\langle O_{\eta_b}\rangle^{1/2}}{N_c}\times \\
& \times \frac{4C_AC_F}{N_c}\sqrt{\frac{m_c}{m_b}}\,e^2g_s^4\left(c_\gamma J_\mu + c_Z\widetilde{J}_\mu\right)\epsilon_\nu^{J/\psi}P_\rho Q_\sigma\,\varepsilon^{\mu\nu\rho\sigma}\times \\
& \times\left(\frac{4im_b^2C_0\left(4m_b^2,m_c^2,2m_b^2-m_c^2+\frac{s}{2};0,0,m_c\right)}{16m_b^4-\left(s-4m_c^2\right)^2}+\right. \\
& -\frac{4im_c^2\left(-4m_b^2+4m_c^2-s\right)C_0\left(m_c^2,2m_b^2-m_c^2+\frac{s}{2},s;m_c,0,m_c\right)}{64m_b^6-16m_b^4(4m_c^2+3s)-4m_b^2(16m_c^4+8m_c^2s-3s^2)+\left(4m_c^2-s\right)^3}+ \\
& -\frac{\pi\left(4m_b^2-4m_c^2+3s\right)}{64m_b^6-16m_b^4(10m_c^2+s)+4m_b^2(32m_c^4-12m_c^2s-s^2)-(2m_c^2-s)(s-4m_c^2)^2}+ \\
& +\frac{i\left(4m_b^2-4m_c^2+3s\right)\ln\left(\frac{2m_c^2}{4m_b^2-4m_c^2+s}\right)}{64m_b^6-16m_b^4(10m_c^2+s)+4m_b^2(32m_c^4-12m_c^2s-s^2)-(2m_c^2-s)(s-4m_c^2)^2}+ \\
& \left.+\frac{4i\sqrt{s(s-4m_c^2)}\ln\left(\frac{\sqrt{s\left(s-4m_c^2\right)}+2m_c^2-s}{2m_c^2}\right)}{-64m_b^6+16m_b^4(12m_c^2+s)+4m_b^2(-48m_c^4+8m_c^2s+s^2)+\left(4m_c^2-s\right)^3}\right),
\end{aligned} \tag{17}$$

$$\begin{aligned}
\mathcal{A}_{QCD}\left(e^+e^- \to \Upsilon\,\eta_c\right) = {} & \frac{\langle O_\Upsilon\rangle^{1/2}\langle O_{\eta_c}\rangle^{1/2}}{N_c}\times \\
& \times \frac{4C_AC_F}{N_c}\sqrt{\frac{m_b}{m_c}}\,e^2g_s^4\left(b_\gamma J_\mu + b_Z\widetilde{J}_\mu\right)\epsilon_\nu^{\Upsilon}P_\rho Q_\sigma\,\varepsilon^{\mu\nu\rho\sigma}\times \\
& \times\left(\frac{4im_c^2C_0\left(m_b^2,4m_c^2,-m_b^2+2m_c^2+\frac{s}{2};m_b,0,0\right)}{16m_b^4-8m_b^2s-16m_c^4+s^2}+\right. \\
& +\frac{4im_b^2\left(4m_b^2-4m_c^2-s\right)C_0\left(m_b^2,-m_b^2+2m_c^2+\frac{s}{2},s;m_b,0,m_b\right)}{64m_b^6-16m_b^4(4m_c^2+3s)-4m_b^2(16m_c^4+8m_c^2s-3s^2)+\left(4m_c^2-s\right)^3}+ \\
& -\frac{\pi\left(-4m_b^2+4m_c^2+3s\right)}{32m_b^6-32m_b^4(4m_c^2+s)+2m_b^2(80m_c^4+24m_c^2s+5s^2)-(s-4m_c^2)^2(4m_c^2+s)}+ \\
& -\frac{i\left(4m_b^2-4m_c^2-3s\right)\ln\left(\frac{2m_b^2}{4m_c^2-4m_b^2+s}\right)}{32m_b^6-32m_b^4(4m_c^2+s)+2m_b^2(80m_c^4+24m_c^2s+5s^2)-(s-4m_c^2)^2(4m_c^2+s)}+ \\
& \left.-\frac{4i\sqrt{s\left(s-4m_b^2\right)}\ln\left(\frac{\sqrt{s\left(s-4m_b^2\right)}+2m_b^2-s}{2m_b^2}\right)}{64m_b^6-48m_b^4(4m_c^2+s)+4m_b^2(48m_c^4+8m_c^2s+3s^2)-(s-4m_c^2)^2(4m_c^2+s)}\right),
\end{aligned} \tag{18}$$

where C_0 is the scalar three-point Passarino-Veltman function `ScalarC0[s1, s12, s2; m0, m1, m2]` defined in Package-X.

As already mentioned, the virtual photon does not decay to the $J/\psi\,\Upsilon$ pair due to the charge parity conservation, while the virtual Z-boson does. The Lorentz structure of this

amplitude is a little bit more complicated than presented in (11) and (12), as contains the additional polarization vector and consists of two components:

$$\mathcal{A}_{EW}\left(e^+e^- \to J/\psi\,\Upsilon\right) = \frac{\langle O_{J/\psi}\rangle^{1/2}\langle O_\Upsilon\rangle^{1/2}}{N_c}\times$$
$$\times\,\frac{e^4\,e_b e_c\sqrt{m_b m_c}}{N_c\cos\theta_w\sin\theta_w\left(s-M_Z^2+i\Gamma M_Z\right)}\,\widetilde{J}_\mu\epsilon^{J/\psi}_{\nu_1}\epsilon^{\Upsilon}_{\nu_2}\varepsilon^{\mu\nu_1\nu_2\sigma}\times$$
$$\times\left(\frac{P_\sigma}{m_c^2\left(4m_b^2-4m_c^2-s\right)}-\frac{Q_\sigma}{m_b^2\left(4m_b^2-4m_c^2+s\right)}\right). \quad (19)$$

The photonic parts of the electroweak amplitudes (11) and (12) turn into each other under simultaneous permutations $m_b \longleftrightarrow m_c$, $e_b \longleftrightarrow e_c$ and $P \longleftrightarrow Q$, as expected (as well as cross sections (15) and (16)). The same applies for the photonic parts of the one loop QCD amplitudes (17) and (18).

It is interesting to note that EW and QCD amplitudes for the VP-pair production have a different asymptotic behaviour:

$$\frac{\mathcal{A}_{QCD}}{\mathcal{A}_{EW}}\Big|_{s\to\infty} \sim \frac{\ln s}{s}. \quad (20)$$

Therefore, asymptotically the total cross section $\sigma_{\text{tot}} = \sigma_{EW} + \sigma_{int} + \sigma_{QCD}$ fall off with the increase of the energy as per

$$\sigma_{\text{tot}} \sim \frac{1}{s^2}\left(1+\mathcal{O}\left(\frac{\ln s}{s}\right)\right), \quad (21)$$

where the main contribution proceeds from the tree level electroweak amplitude. It is interesting to note that the tree level QCD cross section of $J/\psi\,\eta_c$-pair production falls off with energy increasing faster than (21), namely as $1/s^4$, because the latter process is helicity suppressed (see [1] for details).

5. Cross Sections Estimations

The numerical values of parameters used in the calculations are presented in Table 1. The values of NRQCD matrix elements are adopted from the potential model [36]. The strong coupling constant is used within the two loops accuracy:

$$\alpha_S(Q) = \frac{4\pi}{\beta_0 L}\left(1-\frac{\beta_1\ln L}{\beta_0^2 L}\right), \quad (22)$$

where $L = \ln Q^2/\Lambda^2$, $\beta_0 = 11 - \frac{2}{3}N_f$ and $\beta_1 = 102 - \frac{38}{3}N_f$ with $N_f = 5$; the reference value is $\alpha_S(M_Z) = 0.1179$. The appropriate scale $Q = \sqrt{s}$ is chosen for α_s for all investigated energies. For sake of simplicity the fine structure constant is used in Thomson limit: $\alpha = 1/137$.

As it is customary in most studies on quarkonia production within NRQCD, the masses of quarks inside the quarkonium are chosen so that their sum is equal to the quarkonium mass.

Table 1. The parameters used in the calculations. The NRQCD matrix elements are adopted from [36].

m_c = 1.5 GeV	m_b = 4.7 GeV	M_Z = 91.2 GeV	Γ_Z = 2.5 GeV
$\langle O\rangle_{J/\psi} = \langle O\rangle_{\eta_c} = 0.523\ \text{GeV}^3$		$\langle O\rangle_\Upsilon = \langle O\rangle_{\eta_b} = 2.797\ \text{GeV}^3$	$\sin^2\theta_w = 0.23$

The cross sections reference values are given in Table 2. In Figures 2–5 the calculated cross sections and there ratios are performed as functions of $\sqrt{s}$.

In Figure 2, we compare the QCD and EW contributions at low energies (left) and at energies around a Z-mass (right). In Figure 3, the total cross sections including all discussed contributions are demonstrated. In Figure 4, the ratios between QCD and EW contributions are performed. The relative contribution of Z-boson annihilation to the studied processes is shown in Figure 5.

Table 2. The cross section values in fb units at different collision energies.

E, GeV	15	20	30	50	90	180
$J/\psi\ \eta_b$	7.5×10^{-5}	4.4×10^{-5}	7.3×10^{-6}	6.1×10^{-7}	1.2×10^{-5}	4.4×10^{-9}
$\Upsilon\ \eta_c$	1.0×10^{-3}	1.8×10^{-4}	1.1×10^{-5}	4.4×10^{-7}	1.3×10^{-6}	1.1×10^{-9}
$J/\psi\ \Upsilon$	3.3×10^{-8}	4.2×10^{-8}	5.1×10^{-8}	8.4×10^{-8}	2.9×10^{-5}	4.9×10^{-9}

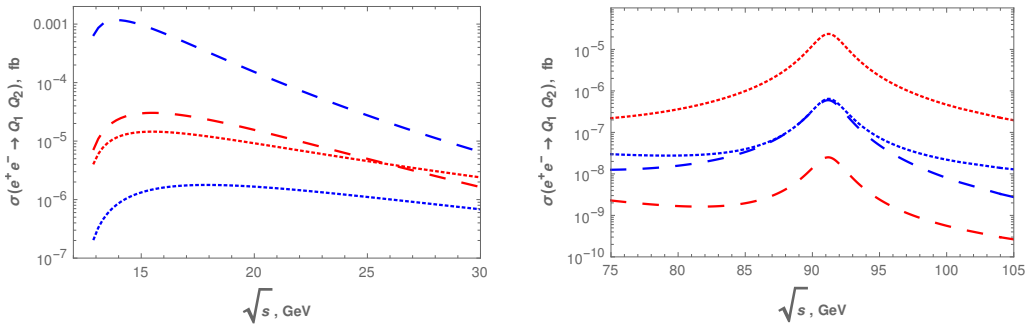

Figure 2. The EW and QCD contributions to the cross sections at low energies (**left**) and near Z pole (**right**): the QCD one loop contribution to $\sigma(J/\psi\ \eta_b)$ (red dashed curve); the EW contribution to $\sigma(J/\psi\ \eta_b)$ (red dotted curve); the QCD one loop contribution to $\sigma(\Upsilon\ \eta_c)$ (blue dashed curve); the EW contribution to $\sigma(\Upsilon\ \eta_c)$ (blue dotted curve).

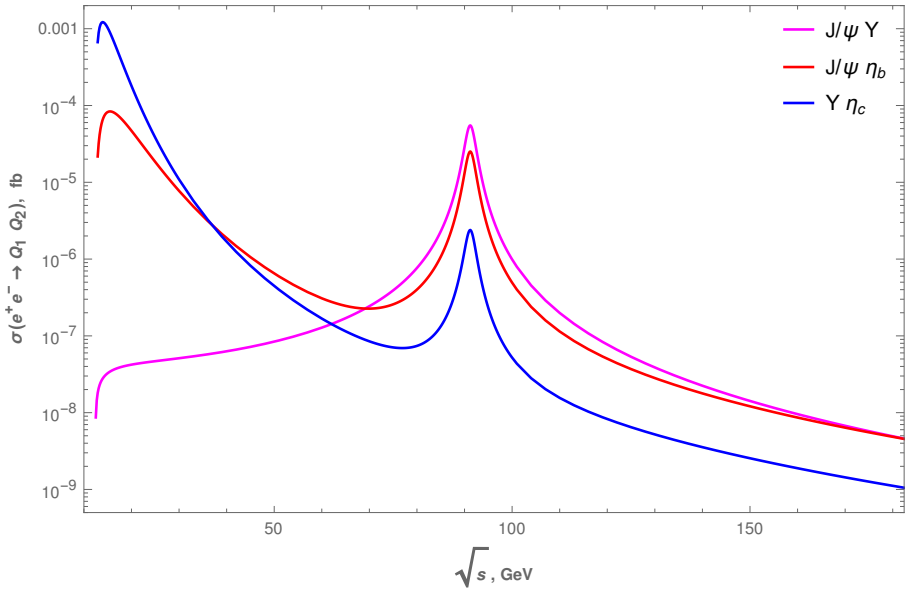

Figure 3. The total cross sections dependence on the collision energy.

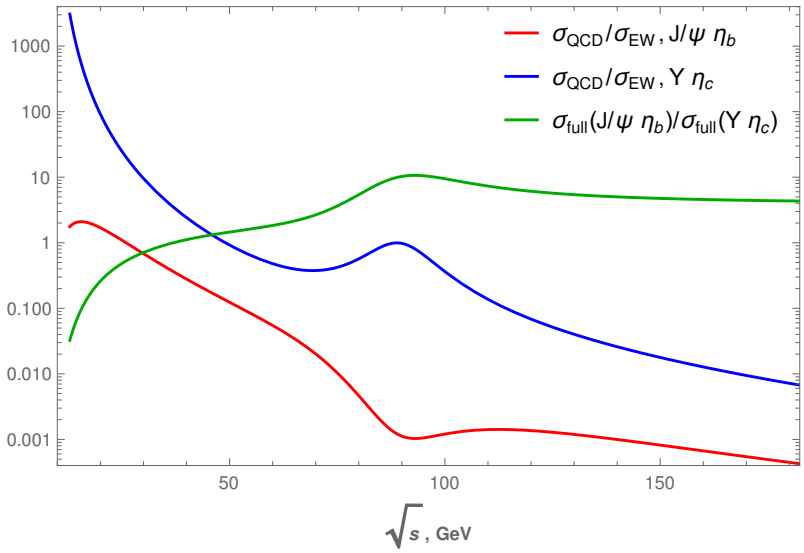

Figure 4. The cross section ratios as a function of the collision energy: $\sigma_{QCD}(J/\psi\,\eta_b)/\sigma_{EW}(J/\psi\,\eta_b)$ (red curve), $\sigma_{QCD}(\Upsilon\,\eta_c)/\sigma_{EW}(\Upsilon\,\eta_c)$ (blue curve), $\sigma_{tot}(J/\psi\,\eta_b)/\sigma_{tot}(\Upsilon\,\eta_c)$ (green curve).

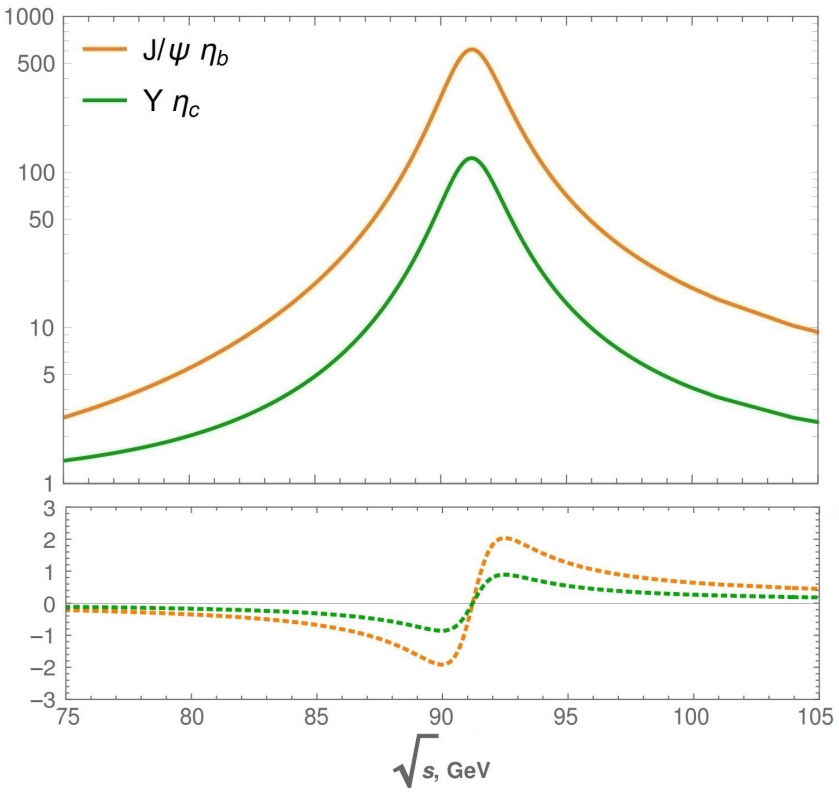

Figure 5. The Z-boson relative contributions as a function of energy: $\sigma_{\gamma+Z}(J/\psi\,\eta_b)/\sigma_{\gamma}(J/\psi\,\eta_b)$ (solid orange curve) and $\sigma_{\gamma+Z}(\Upsilon\,\eta_c)/\sigma_{\gamma}(\Upsilon\,\eta_c)$ (solid green curve), as well as the relative contributions of the interference term between γ and Z: $\sigma^{int}_{\gamma Z}(J/\psi\,\eta_b)/\sigma_{\gamma}(J/\psi\,\eta_b)$ (dashed orange curve) and $\sigma^{int}_{\gamma Z}(\Upsilon\,\eta_c)/\sigma_{\gamma}(\Upsilon\,\eta_c)$ (dashed green curve).

As it can be concluded from the presented Figures 2–5, the QCD and EW subprocesses contribute differently to the total yield of $J/\psi\,\eta_b$ and $\Upsilon\,\eta_c$. In the $J/\psi\,\eta_b$ production, the QCD and EW contributions are comparable at low energies, while the EW contribution dominates near the Z pole. On the contrary, in the $\Upsilon\,\eta_c$ production the QCD and EW

contributions are comparable at energies around Z pole, while at low energies the QCD contribution dominates.

To understand such a strange behaviour, we suggest to look at the problem from another side, and compare the EW contributions with each other, as well as to compare the QCD contributions with each other.

As it can be obtained from the expressions (11), (12), (17) and (18) for EW and QCD amplitudes, the scalar parts of the amplitudes near the Z pole relate as follows:

$$\frac{\mathcal{A}^S_{EW}(e^+e^- \to J/\psi\,\eta_b)}{\mathcal{A}^S_{EW}(e^+e^- \to \Upsilon\,\eta_c)}\Big|_{s\sim m_Z \gg m_b, m_c} \approx \left[\frac{\mathcal{A}^S_{QCD}(e^+e^- \to J/\psi\,\eta_b)}{\mathcal{A}^S_{QCD}(e^+e^- \to \Upsilon\,\eta_c)}\Big|_{s\sim m_Z \gg m_b, m_c}\right]^{-1} \approx$$
$$\approx \frac{(4e_b \sin^2\Theta_w + 1)m_b}{(4e_c \sin^2\Theta_w - 1)m_c} \approx -6. \quad (23)$$

Thus, the ratios between the EW and QCD contributions for the discussed processes near the Z pole are essentially different, and moreover, these ratios are in inverse proportion to each other. Also it can be concluded from Figure 2, that the EW and QCD contributions approximately obey this pattern at all investigated energies: $\sigma_{EW}(J/\psi\,\eta_b)$ is at least by an order of magnitude greater, than $\sigma_{EW}(\Upsilon\,\eta_c)$, whereas $\sigma_{QCD}(J/\psi\,\eta_b)$ is at least by an order of magnitude smaller than $\sigma_{QCD}(\Upsilon\,\eta_c)$.

If one keeps this circumstance in mind, then the behavior of the discussed contributions no longer seems so mysterious. Indeed, if $\sigma_{QCD}(J/\psi\,\eta_b) \sim \sigma_{EW}(J/\psi\,\eta_b)$ at some energy, then at this energy $\sigma_{QCD}(\Upsilon\,\eta_c) \gg \sigma_{EW}(\Upsilon\,\eta_c)$, because $\sigma_{QCD}(\Upsilon\,\eta_c) \gg \sigma_{QCD}(J/\psi\,\eta_b)$ and $\sigma_{EW}(J/\psi\,\eta_b) \gg \sigma_{EW}(\Upsilon\,\eta_c)$. But if at some energy $\sigma_{QCD}(\Upsilon\,\eta_c) \sim \sigma_{EW}(\Upsilon\,\eta_c)$, then at this energy $\sigma_{EW}(J/\psi\,\eta_b) \gg \sigma_{QCD}(J/\psi\,\eta_b)$ for the same reason.

As seen in Figure 3, both the $J/\psi\,\eta_b$-pair and the $\Upsilon\,\eta_c$-pair production cross sections have a maximum near the threshold ($\sqrt{s}_{max}(J/\psi\,\eta_b) \approx 15.6$ GeV and $\sqrt{s}_{max}(\Upsilon\,\eta_c) \approx 14.1$ GeV). The cross section ratios near the maximum take the following values:

$$\frac{\sigma_{QCD}(J/\psi\,\eta_b)}{\sigma_{EW}(J/\psi\,\eta_b)} \sim 2, \qquad \frac{\sigma_{QCD}(\Upsilon\,\eta_c)}{\sigma_{EW}(\Upsilon\,\eta_c)} \sim 10^3, \qquad \frac{\sigma_{tot}(\Upsilon\,\eta_c)}{\sigma_{tot}(J/\psi\,\eta_b)} \sim 15. \quad (24)$$

As already mentioned, near the Z pole, the discussed cross sections behave completely differently:

$$\frac{\sigma_{QCD}(J/\psi\,\eta_b)}{\sigma_{EW}(J/\psi\,\eta_b)} \sim 10^{-3}, \qquad \frac{\sigma_{QCD}(\Upsilon\,\eta_c)}{\sigma_{EW}(\Upsilon\,\eta_c)} \sim 1, \qquad \frac{\sigma_{tot}(\Upsilon\,\eta_c)}{\sigma_{tot}(J/\psi\,\eta_b)} \sim 10^{-1}. \quad (25)$$

As shown in Figure 4 the EW contribution exceeds the QCD contribution starting with some energy both for the $J/\psi\,\eta_b$-pair production and the $\Upsilon\,\eta_c$-pair production in total agreement with (20).

It should be mentioned that the interference between the EW and QCD contributions is strong and positive at all investigated energies. It achieves ∼48% of the total cross section when the EW and QCD cross-sections are compared.

As $J/\psi\,\Upsilon$ pair production goes only via the Z boson exchange it is not surprising that such a process is highly suppressed at low energies against the production of $J/\psi\,\eta_b$-pairs and $\Upsilon\,\eta_c$-pairs (see Figure 3). However at energies higher than 70 GeV the production cross section of $J/\psi\,\Upsilon$ pair becomes greater than the other cross sections: $\sigma(J/\psi\,\Upsilon) > \sigma(J/\psi\,\eta_b) > \sigma(\Upsilon\,\eta_c)$. For example, for the chosen parameter values at $\sqrt{s} = M_Z$ we obtain that

$$\sigma(J/\psi\,\Upsilon) : \sigma(J/\psi\,\eta_b) : \sigma(\Upsilon\,\eta_c) = 22.4 : 10.5 : 1. \quad (26)$$

The Z boson exchange obviously dominates at the Z pole, and also essentially contributes to the production cross section around this pole is such a way that the its contribution to the total cross section value is greater than 20% for energies $\sqrt{s} > 60$ GeV for the

$J/\psi\ \eta_b$-pair production process and for energies in the range 70 GeV $< \sqrt{s} <$ 150 GeV for the Y η_c-pair production process (see Figure 5).

6. Conclusions

The exclusive production of the charmonium-bottomonium pairs ($J/\psi\ \eta_b$, Y η_c and J/ψ Y) has been studied in a single boson e^+e^- annihilation in the interaction energy range from the threshold to $2M_Z$ within the color singlet approximation of NRQCD.

Both $J/\psi\ \eta_b$ and Y η_c productions essentially differ from the thoroughly investigated $J/\psi\ \eta_c$ production, since the main QCD contribution to these processes contains loops and occurs to be comparable in magnitude with the purely electromagnetic contribution ($\mathcal{O}(\alpha^2\alpha_s^4)$ v.s. $\mathcal{O}(\alpha^4)$). This is why the QCD contribution, the electromagnetic contribution and their interference have been studied together. As concerned the J/ψ Y-pair production, in the leading order this process goes via the electroweak Z boson exchange only. The rather simple structure of the studied amplitudes allows to provide the analytical expressions right in the text.

It has been shown in the current study, that the QCD and EW subprocesses contribute differently to the total yield of $J/\psi\ \eta_b$ and Y η_c. In the $J/\psi\ \eta_b$ production the QCD and EW contributions are comparable at low energies, while the EW one highly dominates near the Z pole. On the contrary, in the Y η_c production the QCD contribution highly dominates at low energies, while at energies around the Z pole the QCD and EW contributions are comparable.

It has also been demonstrated that the one-loop QCD amplitude and the electroweak amplitude have a different asymptotic behavior at high energies.

The energy sufficient to produce a charmonium-bottomonium pair can not be achieved at the current e^+e^- experiments. Nevertheless, we believe that the obtained results may be of considerable interest for experiments at future e^+e^- colliders.

Author Contributions: Methodology, validation, writing—original draft preparation, I.B.; conceptualization, supervision, writing—review and editing, A.B.; software, formal analysis, I.B. and E.L.; visualization, E.L. All authors have read and agreed to the published version of the manuscript.

Funding: This research was supported by foundation RFBR, grant No. 20-02-00154 A. I. Belov acknowledges the support from "BASIS" Foundation, grant No. 20-2-2-2-1.

Data Availability Statement: None.

Acknowledgments: Authors would like to thank A. Likhoded, A. Onishchenko and S. Poslavsky for help and fruitful discussions.

Conflicts of Interest: The authors declare no conflict of interest.

Appendix A. $\langle O \rangle$ and $|R(0)|^2$ Values

Table A1. $\langle O \rangle$ and $|R(0)|^2$ (where possible) in GeV^3 for J/ψ, η_c, Y and η_b mesons.

Ref.	$\langle O \rangle_{J/\psi}$ / $\lvert R_{J/\psi}(0)\rvert^2$	$\langle O \rangle_{\eta_c}$ / $\lvert R_{\eta_c}(0)\rvert^2$	$\langle O \rangle_{\Upsilon}$ / $\lvert R_{\Upsilon}(0)\rvert^2$	$\langle O \rangle_{\eta_b}$/$\lvert R_{\eta_b}(0)\rvert^2$
[1]	0.335 ± 0.024	0.297 ± 0.032		
[34]	$0.440^{+0.067}_{-0.055}$	$0.434^{+0.169}_{-0.158}$		
[35]				$3.069^{+0.207}_{-0.190}$
[36]	0.523/1.0952		2.797/5.8588	

Appendix B. Electroweak Amplitudes with $\mathcal{O}\left(\frac{m_q^2}{M_Z^2-4m_q^2}\right)$ Corrections

$$\mathcal{A}_{EW}\left(e^+e^- \to J/\psi\,\eta_b\right) = \frac{\langle O_{J/\psi}\rangle^{1/2}\langle O_{\eta_b}\rangle^{1/2}}{N_c}\times$$
$$\times \frac{-e^4\, e_b e_c}{2N_c m_c\sqrt{m_b m_c}\left(s+4m_c^2-4m_b^2\right)}\left(b_\gamma(1+A_1)J_\mu + b_Z(1+A_2)\widetilde{J}_\mu\right)\epsilon_\nu^{J/\psi}P_\rho Q_\sigma\varepsilon^{\mu\nu\rho\sigma}. \quad \text{(A1)}$$

$$\mathcal{A}_{EW}\left(e^+e^- \to \Upsilon\,\eta_c\right) = \frac{\langle O_\Upsilon\rangle^{1/2}\langle O_{\eta_c}\rangle^{1/2}}{N_c}\times$$
$$\times \frac{e^4\, e_b e_c}{2N_c m_b\sqrt{m_b m_c}\left(s+4m_b^2-4m_c^2\right)}\left(c_\gamma(1+A_3)J_\mu + c_Z(1+A_4)\widetilde{J}_\mu\right)\varepsilon_\nu^\Upsilon P_\rho Q_\sigma\varepsilon^{\mu\nu\rho\sigma}. \quad \text{(A2)}$$

$$\mathcal{A}_{EW}\left(e^+e^- \to J/\psi\,\Upsilon\right) = \frac{\langle O_{J/\psi}\rangle^{1/2}\langle O_\Upsilon\rangle^{1/2}}{N_c}\times$$
$$\times \frac{e^4\, e_b e_c\sqrt{m_b m_c}}{N_c\cos\theta_w\sin\theta_w\left(s-M_Z^2+i\Gamma M_Z\right)}\,\widetilde{J}_\mu\epsilon_{\nu_1}^{J/\psi}\epsilon_{\nu_2}^\Upsilon\varepsilon^{\mu\nu_1\nu_2\sigma}\times$$
$$\times\left(\frac{P_\sigma}{m_c^2\left(4m_b^2-4m_c^2-s\right)}(1+A_5) - \frac{Q_\sigma}{m_b^2\left(4m_b^2-4m_c^2+s\right)}(1+A_6)\right). \quad \text{(A3)}$$

$$A_1 = -\left(\frac{m_c^2}{M_Z^2-4m_c^2}\right)\frac{\left(4e_b\sin^2\theta_w+1\right)\left(4e_c\sin^2\theta_w-1\right)}{4e_b e_c\cos^2\theta_w\sin^2\theta_w},$$

$$A_2 = -\left(\frac{m_c^2}{M_Z^2-4m_c^2}\right)\frac{\left(4e_c\sin^2\theta_w-1\right)\left(\left(4m_b^2-4m_c^2\right)\left(4e_b\sin^2\theta_w+1\right)^2+s\left(8e_b\sin^2\theta_w\left(2e_b\sin^2\theta_w+1\right)+3\right)\right)}{4e_b e_c\cos^2\theta_w\sin^2\theta_w\left(4e_b\sin^2\theta_w+1\right)\left(4m_b^2-4m_c^2+s\right)},$$

$$A_3 = -\left(\frac{m_b^2}{M_Z^2-4m_b^2}\right)\frac{\left(4e_b\sin^2\theta_w+1\right)\left(4e_c\sin^2\theta_w-1\right)}{4e_b e_c\cos^2\theta_w\sin^2\theta_w},$$

$$A_4 = -\left(\frac{m_b^2}{M_Z^2-4m_b^2}\right)\frac{\left(4e_b\sin^2\theta_w+1\right)\left(\left(4m_b^2-4m_c^2\right)\left(4e_c\sin^2\theta_w-1\right)^2-s\left(8e_c\sin^2\theta_w\left(2e_c\sin^2\theta_w-1\right)+3\right)\right)}{4e_b e_c\cos^2\theta_w\sin^2\theta_w\left(4e_c\sin^2\theta_w-1\right)\left(4m_b^2-4m_c^2-s\right)},$$

$$A_5 = -\left(\frac{m_c^2}{M_Z^2-4m_c^2}\right)\frac{\left(4e_b\sin^2\theta_w+1\right)\left(4e_c\sin^2\theta_w-1\right)\left(4m_b^2-4m_c^2+3s\right)}{4e_b e_c\cos^2\theta_w\sin^2\theta_w\left(4m_b^2-4m_c^2+s\right)},$$

$$A_6 = -\left(\frac{m_b^2}{M_Z^2-4m_b^2}\right)\frac{\left(4e_b\sin^2\theta_w+1\right)\left(4e_c\sin^2\theta_w-1\right)\left(4m_b^2-4m_c^2-3s\right)}{4e_b e_c\cos^2\theta_w\sin^2\theta_w\left(4m_b^2-4m_c^2-s\right)}.$$

References

1. Braaten, E.; Lee, J. Exclusive Double Charmonium Production from e^+e^- Annihilation into a Virtual Photon. *Phys. Rev. D* **2003**, *67*, 054007.
2. Abe, K.; Aihara, H.; Asano, Y.; Aulchenko, V.; Aushev, T.; Bahinipati, S.; Zhang, Z.P. Study of double charmonium production in e^+e^- annihilation at s**(1/2) ~ 10.6-GeV. *Phys. Rev. D* **2004**, *70*, 071102. [CrossRef]
3. Aubert, B.; Barate, R.; Boutigny, D.; Couderc, F.; Karyotakis, Y.; Lees, J.P.; Meadows, B.T. Measurement of double charmonium production in e^+e^- annihilations at $\sqrt{s} = 10.6$ GeV. *Phys. Rev. D* **2005**, *72*, 031101. [CrossRef] [CrossRef]
4. Dong, H.R.; Feng, F.; Jia, Y. $O(\alpha_s v^2)$ correction to $e^+e^- \to J/\psi + \eta_c$ at *B* factories. *Phys. Rev. D* **2012**, *85*, 114018. [CrossRef]
5. Li, X.H.; Wang, J.X. $O(\alpha_s v^2)$ correction to J/ψ plus η_c production in e^+e^- annihilation at $\sqrt{s} = 10.6$ GeV. *Chin. Phys. C* **2014**, *38*, 043101, doi:10.1088/1674-1137/38/4/043101. [CrossRef]
6. Feng, F.; Jia, Y.; Sang, W.L. Next-to-next-to-leading-order QCD corrections to $e^+e^- \to J/\psi + \eta_c$ at *B* factories. *arXiv* **2019**, arXiv:1901.08447.
7. Zhang, Y.J.; Gao, Y.j.; Chao, K.T. Next-to-leading order QCD correction to $e^+e^- \to J/\psi + \eta_c$ at $S^{(1/2)}$ = 10.6-GeV. *Phys. Rev. Lett.* **2006**, *96*, 092001,
8. Gong, B.; Wang, J.X. QCD corrections to J/ψ plus η_c production in e^+e^- annihilation at $S^{(1/2)}$ = 10.6-GeV. *Phys. Rev. D* **2008**, *77*, 054028,
9. Bondar, A.; Chernyak, V. Is the BELLE result for the cross section sigma($e^+e^- \to J/\psi + \eta(c)$) a real difficulty for QCD? *Phys. Lett. B* **2005**, *612*, 215–222.
10. Braguta, V.; Likhoded, A.; Luchinsky, A. Excited charmonium mesons production in e+ e- annihilation at s**1/2 = 10.6-GeV. *Phys. Rev. D* **2005**, *72*, 074019,

11. Berezhnoy, A.; Likhoded, A. Quark-hadron duality and production of charmonia and doubly charmed baryons in e+ e- annihilation. *Phys. Atom. Nucl.* **2007**, *70*, 478–484.
12. Braguta, V.; Likhoded, A.; Luchinsky, A. The Processes $e^+e^- \to J/\Psi(\chi(c0)), \Psi(2S)(\chi(c0))$ at $s^{(1/2)}$= 10.6-GeV in the framework of light cone formalism. *Phys. Lett. B* **2006**, *635*, 299–304.
13. Bodwin, G.T.; Kang, D.; Lee, J. Reconciling the light-cone and NRQCD approaches to calculating $e^+e^- \to J/\psi + \eta(c)$. *Phys. Rev. D* **2006**, *74*, 114028,
14. Ebert, D.; Martynenko, A. Relativistic effects in the production of pseudoscalar and vector doubly heavy mesons from e^+e^- annihilation. *Phys. Rev. D* **2006**, *74*, 054008,
15. Berezhnoy, A. Internal motion of massive charmed quarks in double charmonium production in electron-positron annihilation. *Phys. Atom. Nucl.* **2008**, *71*, 1803–1806. [CrossRef]
16. Ebert, D.; Faustov, R.; Galkin, V.; Martynenko, A. Relativistic description of the double charmonium production in e^+e^- annihilation. *Phys. Lett. B* **2009**, *672*, 264–269.
17. Braguta, V.; Likhoded, A.; Luchinsky, A. Study of exclusive processes $e^+e^- \to VP$. *Phys. Rev. D* **2008**, *78*, 074032,
18. Braguta, V. Double charmonium production at B-factories within light cone formalism. *Phys. Rev. D* **2009**, *79*, 074018,
19. Sun, Y.J.; Wu, X.G.; Zuo, F.; Huang, T. The Cross section of the process $e^+e^- \to J/\psi + \eta(c)$ within the QCD light-cone sum rules. *Eur. Phys. J. C* **2010**, *67*, 117–123.
20. Braguta, V.; Likhoded, A.; Luchinsky, A. Exclusive processes of charmonium production and charmonium wave functions. *Phys. Atom. Nucl.* **2012**, *75*, 97–108. [CrossRef]
21. Sun, Z.; Wu, X.G.; Ma, Y.; Brodsky, S.J. Exclusive production of $J/\psi + \eta_c$ at the B factories Belle and Babar using the principle of maximum conformality. *Phys. Rev. D* **2018**, *98*, 094001, doi:10.1103/PhysRevD.98.094001. [CrossRef]
22. LHCb Collaboration. Observation of structure in the J/ψ -pair mass spectrum. *Sci. Bull.* **2020**, *65*, 1983–1993. [CrossRef]
23. Koratzinos, M. FCC-ee accelerator parameters, performance and limitations. *Nucl. Part. Phys. Proc.* **2016**, *273–275*, 2326–2328. [CrossRef]
24. Desch, K.; Lankford, A.; Mazumdar, K.; Mcbride, P.; Michizono, S.; Okada, Y.; Yamamoto, Y. Recommendations on ILC Project Implementation, 2019. Available online: https://hal.archives-ouvertes.fr/hal-02327717/ (accessed on 11 June 2021)
25. Long, K.; Lucchesi, D.; Palmer, M.; Pastrone, N.; Schulte, D.; Shiltsev, V. Muon colliders to expand frontiers of particle physics. *Nat. Phys.* **2021**, *17*, 289–292. [CrossRef]
26. Sirunyan, A.M.; CMS Collaboration. Search for Higgs and Z boson decays to J/ψ or Y pairs in the four-muon final state in proton-proton collisions at s = 13 TeV. *Phys. Lett. B* **2019**, *797*, 134811. [CrossRef]
27. Berezhnoy, A.; Likhoded, A.; Onishchenko, A.; Poslavsky, S. Next-to-leading order QCD corrections to paired B_c production in e^+e^- annihilation. *Nucl. Phys. B* **2017**, *915*, 224–242. [CrossRef]
28. Berezhnoy, A.V.; Belov, I.N.; Poslavsky, S.V.; Likhoded, A.K. One-loop corrections to the processes $e^+e^- \to \gamma, Z_0 \to J/\psi\, \eta_c$ and $e^+e^- \to Z_0 \to J/\psi\, J/\psi$. *arXiv* **2021**, arXiv:2101.01477.
29. Karyasov, A.A.; Martynenko, A.P.; Martynenko, F.A. Relativistic corrections to the pair B_c-meson production in e^+e^- annihilation. *Nucl. Phys. B* **2016**, *911*, 36–51.
30. Berezhnoy, A.V.; Martynenko, A.P.; Martynenko, F.A.; Sukhorukova, O.S. Exclusive double B_c meson production from e^+e^- annihilation into two virtual photons. *Nucl. Phys. A* **2019**, *986*, 34–47.
31. Dorokhov, A.E.; Faustov, R.N.; Martynenko, A.P.; Martynenko, F.A. Photonic production of a pair of B_c mesons. *Phys. Rev. D* **2020**, *102*, 016027,
32. Belov, I.N.; Berezhnoy, A.V.; Dorokhov, A.E.; Likhoded, A.K.; Martynenko, A.P.; Martynenko, F.A. Higgs boson decay to paired B_c: Relativistic and one-loop corrections. *arXiv* **2021**, arXiv:2105.02207.
33. Bodwin, G.T.; Braaten, E.; Lepage, G.P. Rigorous QCD analysis of inclusive annihilation and production of heavy quarkonium. *Phys. Rev. D* **1995**, *51*, 1125–1171.
34. Bodwin, G.T.; Chung, H.S.; Kang, D.; Lee, J.; Yu, C. Improved determination of color-singlet nonrelativistic QCD matrix elements for S-wave charmonium. *Phys. Rev. D* **2008**, *77*, 094017. [CrossRef]
35. Chung, H.S.; Lee, J.; Yu, C. NRQCD matrix elements for S-wave bottomonia and $\Gamma[\eta_b(nS) \to \gamma\gamma]$ with relativistic corrections. *Phys. Lett. B* **2011**, *697*, 48–51. [CrossRef]
36. Eichten, E.J.; Quigg, C. Quarkonium wave functions at the origin: An update. *arXiv* **2019**, arXiv:1904.11542.
37. Hahn, T. Generating Feynman diagrams and amplitudes with FeynArts 3. *Comput. Phys. Commun.* **2001**, *140*, 418–431. [CrossRef]
38. Shtabovenko, V.; Mertig, R.; Orellana, F. FeynCalc 9.3: New features and improvements. *Comput. Phys. Commun.* **2020**, *256*, 107478. [CrossRef]
39. Feng, F. `Apart`: A Generalized Mathematica Apart Function. *Comput. Phys. Commun.* **2012**, *183*, 2158–2164.
40. Smirnov, A. Algorithm FIRE—Feynman Integral REduction. *J. High Energy Phys.* **2008**, *10*, 107. [CrossRef] [CrossRef]
41. Patel, H.H. Package-X 2.0: A Mathematica package for the analytic calculation of one-loop integrals. *Comput. Phys. Commun.* **2017**, *218*, 66–70. [CrossRef]
42. Laporta, S. High precision calculation of multiloop Feynman integrals by difference equations. *Int. J. Mod. Phys. A* **2000**, *15*, 5087–5159. [CrossRef]